Chapter 8

Bio-Optical Modeling in a Tropical Hypersaline Lagoon Environment

Igor Ogashawara, Marcelo P. Curtarelli, Carlos A. S. Araujo and José L. Stech

Additional information is available at the end of the chapter

http://dx.doi.org/10.5772/61869

Abstract

In this chapter, we attempted to present an overview of the use of remote sensing to monitor water quality parameters, mainly chlorophyll-*a* (chl-*a*) and turbidity. We summarized the main concepts of bio-optical modeling and presented a case study of the application of the Hyperspectral Imager for the Coastal Ocean (HICO) for the monitoring of water quality in a tropical hypersaline aquatic environment. Using HICO, we evaluated a set of different semi-empirical bio-optical algorithms for chl-*a* and turbidity estimation developed for inland and oceanic waters in the Araruama Lagoon, RJ, Brazil, which is an extreme environment due to its high salinity values. We also developed an empirical algorithm for both water quality parameters and compared the performances. Results showed that for chl-*a* estimation all models have a low performance with a normalized root mean square error (NRMSE) varying from 24.13 to 30.46. For turbidity, the bio-optical algorithms showed a better performance with the NRMSE between 15.49 and 28.04. Overall, these results highlight the importance of including extreme environments, such as the Araruama Lagoon, on the validation of bio-optical algorithms as well as the need for new orbital hyperspectral sensors which will improve the development of the field.

Keywords: Water quality, chlorophyll-*a*, turbidity, bio-optical modeling

1. Introduction

Earth Observations from space began in August, 1972, with the launch by National Aeronautics and Space Administration (NASA) of the Earth Resources Technology Satellite (ERTS-1) [1]. However, the use of remote sensing techniques to monitor inland water quality parameters such as chlorophyll-a (chl-*a*), total suspended solids (TSS) and turbidity only started to be extensively used in the past two decades with the development of bio-optical algorithms as

well as the new hyperspectral and multispectral sensors. The use of optical remote sensing enables spatiotemporally comprehensive assessment of optical properties of the water column.

Water column optical properties are grouped into inherent optical properties (IOPs) and apparent optical properties (AOPs). IOPs are related to those properties that depend only upon the environment, thus, they are independent of the environment light field. The two most essential IOPs are the total absorption coefficient (a) and the total scattering coefficient (b) and the sum of both coefficients is the attenuation coefficient (k). AOPs, on the other hand, are those properties that depend on the environment and also on the directional structure of the environment light field. AOPs are also used as descriptors of a water body due to their regular features and stability. The most common AOPs are the irradiance reflectance (R), the remote-sensing reflectance (R_{rs}) and various diffuse attenuation functions [2]. A list of the most common IOPs and AOPs used in the literature is shown in Table 1.

Quantity	Units (SI)	Simbology
	Inherent Optical Properties	
Absorption coefficient	m^{-1}	a
Volume scattering function	m^{-1} sr^{-1}	β
Scattering phase function	m^{-1}	$\beta\sim$
Scattering coefficent	m^{-1}	b
Backscatter coefficient	m^{-1}	b_b
Beam attenuation coefficient	m^{-1}	c
Single-scattering albedo	-	ω_0
	Apparent Optical Properties	
Irradiance reflectance (ratio)	-	R
Remote sensing reflectance	sr^{-1}	R_{rs}
Remote sensing reflectance (sub)	sr^{-1}	r_{rs}
Attenuation coefficients:		
of radiance $L(z, \theta, \varphi)$	m^{-1}	$K(\theta, \varphi)$
of downwelling irradiance $E_d(z)$	m^{-1}	K_d
of upwelling irradiance $E_u(z)$	m^{-1}	K_u
of Photosynthetic Active Radiation (PAR)	m^{-1}	$KPAR$

Table 1. IOPs and AOPs commonly used in optical hydrology

http://dx.doi.org/10.5772/61869

Based on the interaction among AOPs and IOPs, absorption, scattering and attenuation properties of the water column are retrieved from proximal, aerial or orbital measurements of the solar spectrum mainly in the visible and near-infrared (NIR) spectral range. These optical properties allow the estimation of different water quality parameters such as: primary production, turbidity, eutrophication, particulate and dissolved carbon contents or the assessment of currents and algal blooms [3]. The relation among all these optical properties as well as the equipment to measure them were developed by oceanographers based on the modeling of downwelling solar and sky radiation spectra with the air–water interface and the subsurface aquatic absorption and scattering centers. Studies such as [4–8], among numerous others, established the main theory of the field before or around the launch of ERTS-1.

The first application of the theories of hydrologic optics was described by [9], which used a Monte Carlo simulation of the radiative transfer equation to relate the AOPs to the IOPs in oceanic waters containing optically active constituents, molecular water and chl-*a*. For inland waters, the first application of the hydrologic optics theories was developed for Lake Ontario, Canada, by a Monte Carlo simulation of the radiative transfer equation and non-linear multivariate optimization analyses [10]. These applications started a relatively new area for remote sensing applications known as bio-optical modeling, which focus on the use of the radiative transfer theory to derive optical properties or biological activity in the water column [2]. In [11], a classification of the bio-optical modeling products (algorithms) was proposed by describing five different types of algorithms: empirical, semi-empirical, semi-analytical, quasi-analytical and analytical. In this classification, the first two types (empirical and semi-empirical) and the last one (analytical) are usually used to estimate the biological activity from AOPs using more statistical methods, while the other two types (semi-analytical and quasi-analytical) are used to estimate IOPs from AOPs using the radiative transfer theory.

The development of bio-optical algorithms usually starts by collecting in situ limnological data as well as hyperspectral R_{rs} using a proximal sensor. The use of a hyperspectral sensor is appropriated to explore absorption peaks, which are very narrow to be identified by a multispectral one, to develop an algorithm. However, the ultimate goal for a bio-optical algorithm is to test its applicability on orbital sensors in order to become an important monitoring tool. Two of the most used satellite sensors to monitor water quality are the medium resolution imaging spectrometer (MERIS) and moderate resolution imaging spectroradiometer (MODIS); both sensors provide the necessary spectral bands; however, their coarse spatial resolution makes them suitable only for very large aquatic systems. Despite the limitation on their spatial resolution, several research focus on the use of these two sensors for the monitoring of water quality parameters in inland water. Ref. [12] evaluated the performance of different chl-*a* semi-empirical algorithms developed, especially for MERIS on a tropical reservoir in Brazil, and in [13] the authors developed a series of steps to improve the estimation of chl-*a* and cyanobacteria blooms in inland and near-coastal waters based on the MERIS imagery. For MODIS, empirical [14] and semi-empirical [15–17] algorithms have been developed for the monitoring of different water quality parameters.

To overpass the problem of the spatial resolution and to keep a good spectral resolution, hyperspectral airborne sensors have been used to monitor the quality of inland waters. One of the most common airborne hyperspectral sensor used to monitor water quality parameters is the airborne imaging spectrometer for application (AISA), which is a push-broom system that collect spectral-radiance data (upwelling radiance and downwelling solar irradiance) in the visible and NIR range of the electromagnetic spectrum (approximately from 392 to 982 nm with a bandwidth of 7–8 nm). From an altitude of 1,000 m, this sensor has a spatial resolution of 1 m, surpassing the problems caused by medium to low spatial resolutions found in orbital sensors. In [18], AISA imagery was used to estimate chl-*a* and phycocyanin (PC) concentrations in a mesotrophic reservoir in Central Indiana, USA, based on a series of semi-empirical algorithms. In [19], the authors used the same imagery from the previous study [18] to apply a quasi-analytical algorithm and spatialize the chl-*a*, backscattering (b_b) and *a*. In [20], AISA imagery was used to measure chl-*a*, suspended solids, turbidity and other measures of water clarity from major rivers of Minnesota, USA. Although the use of airborne hyperspectral sensors showed to be an alternative to the development of bio-optical algorithms, because of the expenses of the acquisition and low temporal availability, airborne sensors have not been highly used for water quality monitoring.

An orbital hyperspectral sensor could be the solution for the high costs of flying an airborne sensor, and this was accomplished by the launch of Hyperion, in 2000. However, this sensor was not used in a water quality research because of its signal-to-noise ratio which was very low [21], and also because of its unreliability caused by problems such as radiometric instability. An alternative for the acquisition of hyperspectral images with a medium spatial resolution was the hyperspectral imager for the coastal ocean (HICO), a hyperspectral sensor with 87 spectral bands covering the visible and NIR range (400–900 nm) on-board of the International Space Station (ISS). HICO acquired programmed images from September 2009 to September 2014 with a spatial resolution of 90 m, higher than MERIS (300 m) and MODIS (250, 500 and 1000 m). Since HICO was a sensor developed for the monitoring of aquatic environments, several researches used it to monitor several parameters such as: seagrass and algae mapping [22], cloud removal [23], red tide detection [24], improved chl-*a* detection [25] and harmful cyanobacteria bloom detection [26]. These studies showed strong relationships between these aquatic constituents and reflectance data which could be used to monitor water quality. They also highlight the importance of having an orbital hyperspectral sensor with a high signal-to-noise ratio to improve the development of bio-optical algorithms for inland and coastal waters. The bio-optical modeling of water quality parameters can be used as a complement to conventional monitoring programs which are usually based on sampling and analyzing of few spots in the aquatic system. Moreover, traditional monitoring programs are costly and time-consuming [27], while bio-optical modeling can quickly provide a synoptic view of the environment.

1.1. Hypothesis

Bio-optical algorithms developed for inland or deep ocean waters are unable to uptake empirical algorithms developed especially for extreme environments.

http://dx.doi.org/10.5772/61869

1.2. Objectives

In this chapter, we attempted to present an overview of the application of bio-optical algorithms to monitor water quality parameters as well as to assess chl-*a* and turbidity from a hypersaline tropical lake (Araruama Lagoon) in Rio de Janeiro, Brazil, using HICO imagery and different bio-optical algorithms. A secondary goal of this chapter was to evaluate the performance of bio-optical algorithms for the estimation of chl-*a* and turbidity in an extreme aquatic system such as the Araruama Lagoon.

2. Study site

The Araruama Lagoon is a hypersaline coastal lagoon located in the central coast of Rio de Janeiro State, Southeastern Brazil, between latitudes 22°50′S and 22°57′ S and the longitudes 42°00′ W and 42°44′ W. It is situated in a micro-region called "Região dos Lagos", around 120 km from Rio de Janeiro City (Figure 1a,b). This region is densely populated showing a population density around 268 habitants per square kilometer [28]. The lagoon area encompasses five municipalities: Araruama, Arraial do Cabo, Cabo Frio, Iguaba Grande, São Pedro da Aldeia and Cabo Frio (see Figure 1c).

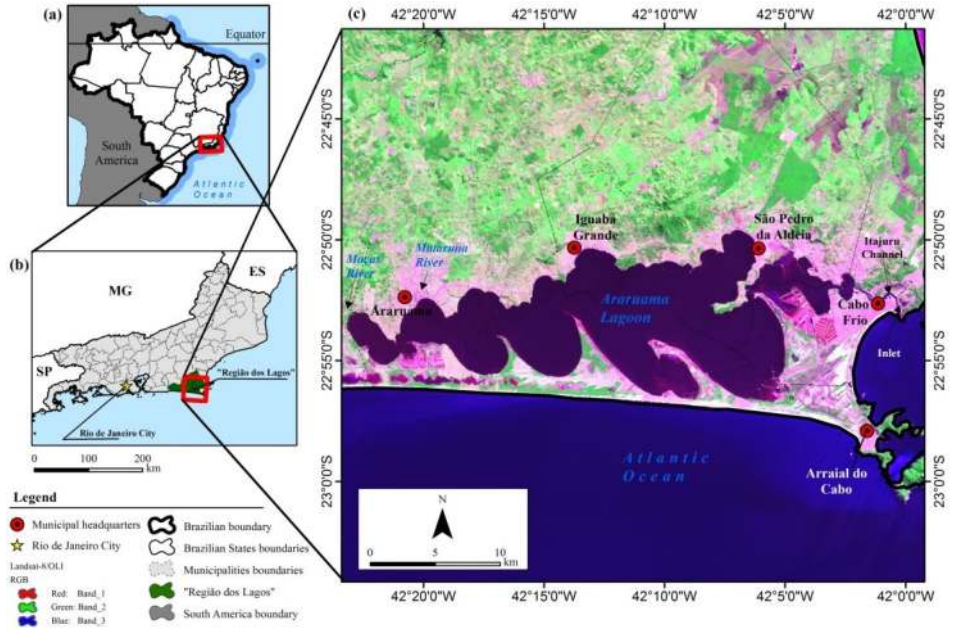

Figure 1. The Araruama Lagoon: (a) Location in Southeastern Brazil, (b) position within the Rio de Janeiro State, and (c) orbital image of the Araruama Lagoon acquired on 1st August 2015 by the Operational Land Imager (OLI) onboard Landsat-8 satellite. The satellite images are presented in false color composition R4G5B2.

From the morphological point view, the Araruama Lagoon consists of a series of elongated spits and shallow embayment presenting a longitudinal elongated shape with around 35 km in length and a mean width of 8 km; the maximum width is around 13 km. The surface area is around 220 km^2 and the depth ranges from 1 to 17 m; the mean depth is around 3 m [29]. The only connection between the Araruama Lagoon and sea, the Itajuru Channel, is located in the Cabo Frio City, Northeastern portion of the lagoon (see Figure 1c). The drainage basin covers around 320 km^2, and permanent sources of freshwater come from Moças River and Mataruna River, in the Western portion of the Lagoon (see Figure 1c); the two rivers present a combined discharge of 1 m^3/s [30].

The salinity of the Araruama Lagoon ranges from 35 to 43 practical salinity unit (psu) in the Itajuru Channel and from 46 to 56 psu in the main body of the Lagoon, being the salinity mainly balanced by the climatology of the area [29]. According to the Köppen-Ginger classification scheme [31], the climate in the region can be classified as Tropical Monsoon (Am) with rainfall ranging between 36 (August) and 101 mm per month (December) and the air temperature ranging from 21 (August) and 25.4°C (February–March) along the year ([32], see Figure 2); the mean annual precipitation is 771 mm per year and the mean air temperature is around 23°C.

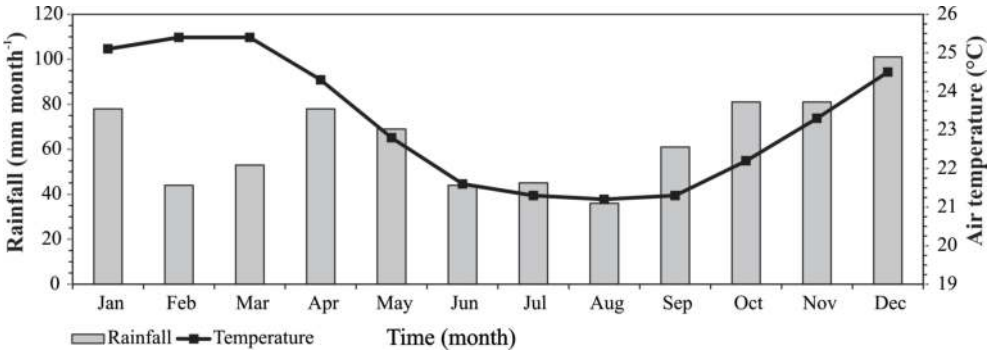

Figure 2. Climatological (1961–1990) monthly rainfall and air temperatures in the Araruama Lagoon region. Data registered on Cabo Frio meteorological station (Lat. -22.98°; Long. 42.03°). Source [32].

The water quality in the Araruama Lagoon has changed over the time, showing an increasing eutrophication along the past few years as a result of the increasing urban growth in the Região dos Lagos [33]. According to the Trophic State Index (TSI) classification scheme proposed by [34], the Araruama Lagoon can be classified as eutrophic environment, with an average total phosphorous concentration around 0.09 mg/L and the average chl-*a* concentration around 11.7 μg/L [35]. Cyanobacteria (*Synechococcus* sp, *Oscillatoria* sp and *Synechocystis* sp) is the dominant community in the water column along the year (around 84% of the total cell count), followed by Diatomaceous (around 7% of the total cell count) and Dinoflagellates (around 5% of the total cell count) [36].

http://dx.doi.org/10.5772/61869

3. Materials and methods

3.1. Remote sensing data

HICO imageries of Araruama Lagoon were acquired from HICO's website database at Oregon State University (OSU) [37]. The acquisition of the images over Araruama Lagoon occurred from 2011 to 2013, where only images without cloud cover over the lagoon were selected. HICO images are available with a Level 1B of processing, which corresponds to the radiance in the top of the atmosphere (L_{TOA}) given in $Wm^{-2}\mu m^{-1}sr^{-1}$ after the application of a division factor of 50. Table 2 lists the HICO imagery with clear sky over the Araruama Lagoon.

Year	Julian day	Image Name
2011	220	iss.2011220.0808.120519.L1B.GLT_Habitat_Brazil.v04.7594.20110809180058.100m.hico
2012	037	iss.2012037.0206.112051.L1B.GLT_Habitat_Brazil.v04.9365.20120206182247.100m.hico
2012	040	iss.2012040.0209.100728.L1B.GLT_Habitat_Brazil.v04.9394.20120209193848.100m.hico
2012	094	iss.2012094.0403.122511.L1B.GLT_Habitat_Brazil.v04.9907.20120403190851.100m.hico
2012	282	iss.2012282.1008.094232.L1B.GLT_Habitat_Brazil.v04.11631.20121009174522.100m.hico
2013	152	iss.2013152.0601.114032.L1B.GLT_Habitat_Brazil.v04.13707.20130603175752.100m.hico
2013	215	iss.2013215.0803.110724.L1B.GLT_Habitat_Brazil.v04.14303.20130805151206.100m.hico
2013	279	iss.2013279.1006.094546.L1B.GLT_Habitat_Brazil.v04.14826.20131007170614.100m.hico

Table 2. List of clear sky HICO images over Araruama Lagoon

All these images were atmospherically corrected by the Second Signal in the Solar Spectrum (6S) implementation of Tafkaa algorithm [38]. Tafkaa is a radiative transfer algorithm developed mainly for applications in the field of oceanic hyperspectral remote sensing, and it is based on an earlier code named ATmospheric REMoval (ATREM) [39]. Tafkaa is available for processing HICO images online via a web tool [37], with prior registration. For the atmospheric correction over the Araruama Lagoon, the aerosol model was set to "maritime" and the atmospheric model was set to "tropical", since these characteristics seem to be the more appropriate for the study site. The final products of this process are delivered in units of R_{rs}, sr^{-1}, and the spectra from the 12 sampling points of the Inter-Municipal Consortium Lagos São João [35] were obtained for the bio-optical modeling.

3.2. Limnological data

Chl-*a* (μg/L) and turbidity (NTU) data were acquired from the reports from the Inter-municipal Consortium Lagos São João, which are available at [35]. This consortium collects monthly data from 12 sampling points in the Araruama Lagoon and has the goal to propose and execute actions to recover the environment in the watershed of three different lagoons (Jaconé,

Saquarema e Araruama) in Rio de Janeiro State, Brazil. Reports matching the HICO imagery (i.e., field campaigns that were carried out on the nearest date as possible as the images acquisition, Table 2) were used to acquire chl-*a* and turbidity data and a total of 87 useful sampling locations were found. These data were divided into two datasets: calibration (53 sampling points using data from 2011 to 2012) and the validation (34 sampling points using data from 2013). Figure 3 shows box-plots to access the statistical distribution of the chl-*a* (μg/L) and turbidity (NTU) values from Araruama Lagoon that were used to calibrate and validate the bio-optical algorithms.

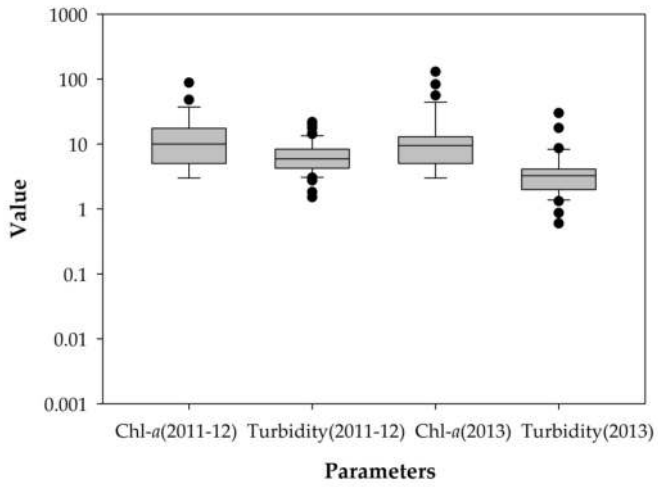

Figure 3. Box-plots of chl-*a* (μg/L) and turbidity (NTU) values used for calibration (2011–12) and for validation (2013) of the bio-optical algorithms.

3.3. Bio-optical algorithms

Several empirical and semi-empirical bio-optical algorithms for chl-*a* and turbidity have been developed in the past decade. Since HICO is a hyperspectral sensor, it is possible to apply several bio-optical algorithms which use different spectral bands. For the estimation of chl-*a* spectral features such low reflectance (troughs) at ~430 nm and ~670 nm caused by the absorption of chl-*a* and a phytoplankton scattering peak at ~700 nm are commonly used in the development of semi-empirical algorithms. The combination of these spectral features makes the ratio of between R_{rs} around 700 and 670 nm [40] widely used for bio-optical algorithm for estimating chl-*a* concentration in turbid waters. There are other algorithms that employ slight variations of this ratio, such as the three band algorithm [41] which uses a third band to minimize the effect of scattering which should be a spectral band with minimal absorption (usually around 750 nm). Another variation is the four band algorithm [42] which includes a spectral band located near 700 nm to enhance the minimization of scattering of suspended matter at the NIR and the absorption by water. Recently, a Normalize Difference Chlorophyll

http://dx.doi.org/10.5772/61869

Index (NDCI) [43] was proposed to estimate chl-*a* concentrations in turbid waters and also used the relationship between 700 and 670 nm. All these algorithms were proposed to estimate chl-*a* concentration in turbid waters; however, for deep ocean waters chl-*a* can also be estimated by algorithms based on band ratios focusing on the chl-*a* absorption around 430 nm and the scattering of particulate matter around 560 nm [44].

Name	Algorithm	Reference
	Chl-a Algorithms	
2BDA	$\frac{R_{rs}(band_{54})}{R_{rs}(band_{47})}$	[40]
3BDA	$\frac{R_{rs}(band_{62})}{\left[R_{rs}(band_{47}) - R_{rs}(band_{54})\right]}$	[41]
4BDA	$\left\{\left[\frac{1}{R_{rs}(band_{46})}\right] - \left[\frac{1}{R_{rs}(band_{51})}\right]\right\} / \left\{\left[\frac{1}{R_{rs}(band_{60})}\right] - \left[\frac{1}{R_{rs}(band_{54})}\right]\right\}$	[42]
NDCI	$\frac{\left[R_{rs}(band_{54}) - R_{rs}(band_{47})\right]}{\left[R_{rs}(band_{54}) + R_{rs}(band_{47})\right]}$	[43]
OC3A	$\frac{R_{rs}(band_{8})}{R_{rs}(band_{27})}$	[44]
OC3B	$\frac{R_{rs}(band_{16})}{R_{rs}(band_{27})}$	[44]
OC3C	$\frac{R_{rs}(band_{20})}{R_{rs}(band_{27})}$	[44]
	Turbidity Algorithms	
1BDA	$R_{rs}(band_{43})$	[45]
2BDA	$\frac{R_{rs}(band_{81})}{R_{rs}(band_{43})}$	[46]
LSBA	$R_{rs}(band_{15}) + R_{rs}(band_{28})$	[47]

Table 3. List of bio-optical algorithms for chl-*a* and turbidity using HICO spectral bands

Turbidity is usually identified by the high reflectance in the red and NIR spectral bands and is usually correlated to the total suspended solids concentration. Therefore, bio-optical algorithms for TSS can be used to estimate turbidity. The simplest algorithm uses the R_{rs} at 645 nm to estimate turbidity [45]; however, other algorithms were also proposed to estimate turbidity using the relationship between NIR and red spectral bands, such as the band ratio proposed by [46]. Another algorithm to estimate turbidity is based on the sum of R_{rs} in the blue and green spectral bands [47]. However, most of the algorithms were developed for inland, coastal or oceanic waters and have not been applied in extreme environments such as the hypersaline Araruama Lagoon. Table 3 lists the published semi-empirical bio-optical algo-

rithms for chl-*a* and turbidity evaluated in this chapter. The algorithms in this list are expressed according to the 87 HICO's spectral bands.

3.4. Bio-optical algorithm development

Since the Araruama Lagoon is a hypersaline aquatic system, and the bio-optical algorithms listed in the previous section were develop for fresh or oceanic waters, we developed two empirical algorithms for the estimation of chl-*a* and turbidity. The development of these empirical algorithms was conducted by calculating the correlation among different band ratios and the concentrations of chl-*a* and turbidity values. To perform this analysis, we used a web tool named Interactive Correlation Environment (ICE) described by [48] and available at [49]. This web tool builds a two-dimensional correlation plot of the HICO's R_{rs} and its relation to the interested limnological parameter (i.e., chl-*a* or turbidity). The two-dimensional color correlation plot can cover all possible band ratios, which in the HICOs case is equal to 7,569 possible combinations, making it a useful tool for the analysis of hyperspectral measurements with a large number of spectral bands.

3.5. Bio-optical algorithms comparison

As described in Section 3.2, the data were divided in calibration (2011–12, 53 sampling points) and validation (2013, 34 sampling points) datasets. For the calibration dataset, a linear regression analysis was computed by the values of slope and intercept for each of the algorithms listed on Table 3 plus the two empirical algorithms developed by the use of ICE. The determination coefficient (R^2) was also computed and the algorithms that had the highest R^2 values were used for validation.

The validation process was computed by analysing a scatter plot between the measured and the estimated values of chl-*a* and turbidity. For chl-*a*, the concentration values were transformed to log (chl-*a*) and for the turbidity, no transformation was needed. We also used errors estimators such as the root mean squared error (RMSE in μg/L or NTU, equation 1) and the normalized root mean squared error (NRMSE, equation 2) to evaluate the performance of the bio-optical algorithms after their calibration.

$$RMSE = \sqrt{\frac{1}{n}\sum_{i=1}^{n}\left(y_i - x_i\right)^2} \tag{1}$$

$$NRMSE = \frac{RMSE}{\left(y_{i,max} - y_{i,min}\right)} \tag{2}$$

where: y_i and x_i are the measured and predicted chl-*a*/turbidity values, respectively. In the *i*-th sample, $y_{i,\max}$ and $y_{i,\min}$ are the maximum and minimum chl-*a*/turbidity values, respectively.

http://dx.doi.org/10.5772/61869

4. Results and discussions

4.1. ICE's results

To compute the two-dimensional color correlation plot, the R_{rs} spectra were extracted from HICO imagery over the sampling locations in the Araruama Lagoon (Figure 4). Figure 4 presents the R_{rs} spectra of the calibration (Figure 4A) and validation (Figure 4B) datasets. Both datasets presented spectral features of an eutrophic water, with a high reflectance peak in the green range around 550 nm, a trough near 620 nm, another trough around 665 nm and a peak in the NIR around 700 nm. The reflectance peak around 550 nm represents the minimal absorption of all algal pigments and the scattering of non-organic suspended matter and phytoplankton cell walls [50]. The trough around 620 nm occurs due to the absorption of phycocyanin, a phycobillin presented in inland water cyanobacteria [51–52]. The trough around 665 nm is due to the absorption of chl-*a* in the red range of the spectrum and the peak around 700 nm is also dependable of the chl-*a* since it represents the scattering of the suspended matter which includes algal biomass [53]. The two-dimensional color correlation plot was computed using the R_{rs} from the calibration dataset as well as the limnological dataset presented in Section 3.2.

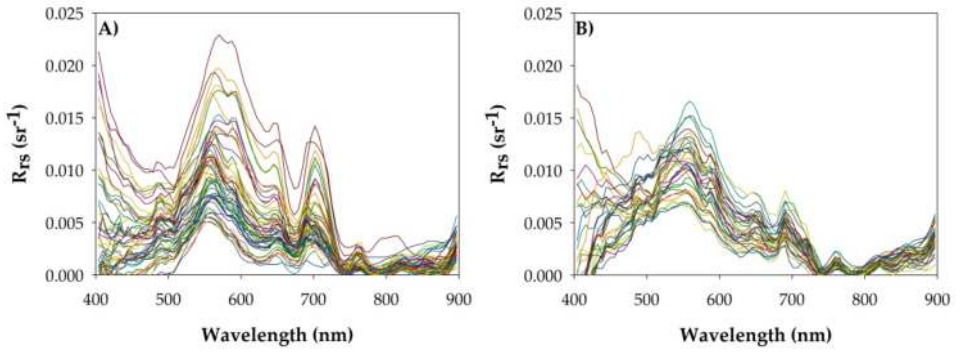

Figure 4. R_{rs} spectra from HICO imagery after atmospheric correction. A) R_{rs} spectra from 2011 and 2012 used for the calibration; B) R_{rs} spectra from 2013 used for the validation.

The use of ICE generates two different two-dimensional color correlation plots, one for chl-*a* (Figure 5A) and one for turbidity (Figure 5C). Using the filtering tool implemented in ICE, it was possible to select the band ratio that gives the highest R^2 for each of the parameters. Figure 5B shows the filtered plot for chl-*a* estimation which highlights only the band ratios with high R^2, Figure 5D shows the same filtered plot for the turbidity. Since the choices of spectral bands are only based on the statistical estimators among all possible band ratios, the algorithms

derived from this web tool can be classified as empirical, and does not have a biophysical background to support the spectral bands used in each band ratio.

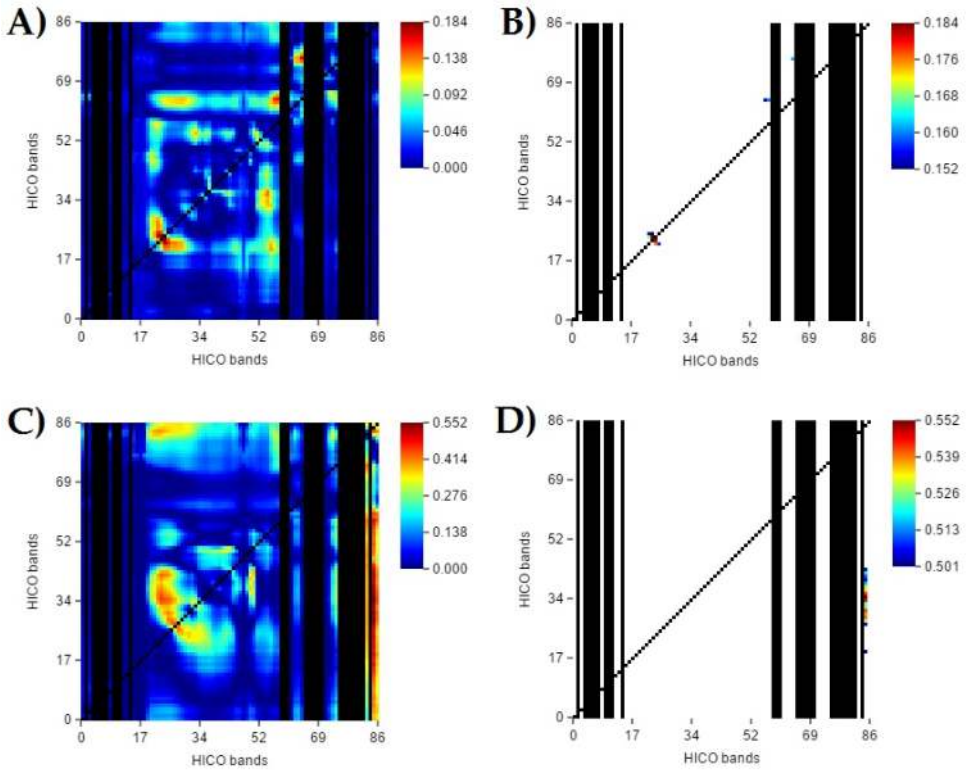

Figure 5. Two-dimensional color correlation plots produced by the web tool. (A) For chl-*a* estimation; (B) After the filtering the chl-*a* plot; (C) For turbidity estimation; (D) After the filtering the turbidity plot.

For chl-*a* the best R^2 was found in correlation to the ratio between band 26 and band 25 which in wavelengths are around 547 and 541 nm, respectively. This relationship is totally empirical and since both bands are very close to each other, the value from this ratio is probably close to 1. For the turbidity band ratio, ICE selected the ratio between band 36 and band 87, which respectively corresponds to 604 and 896 nm. Although it is an empirical model, these two bands can be justified by the fact in both wavelengths the suspended matter will have a high scattering, and if the suspended matter is high, the turbidity will also be high. The formulation and name of these two empirical bio-optical algorithms were described in Table 4.

http://dx.doi.org/10.5772/61869

Name	Parameter	Algorithm
EMPC	Chl-*a*	$\frac{R_{rs}(band_{26})}{R_{rs}(band_{25})}$
EMPT	Turbidity	$\frac{R_{rs}(band_{36})}{R_{rs}(band_{87})}$

Table 4. Empirical algorithms for chl-*a* and turbidity developed using ICE

4.2. Algorithms performances

4.2.1. Calibration

Calibration was conducted using the semi-empirical (Table 3) and empirical (Table 4) bio-optical algorithms. Linear regressions were computed between bio-optical algorithms and chl-*a* and TSS values; the R^2, slope and intercept from each of the regressions were shown in Table 5. For the calibration of chl-*a* algorithms, all the algorithms showed a poor performance with the highest R^2 value of 0.087 found by applying EMPC to the calibration dataset. The other high values of R^2 were found by using OC3C (0.065), OC3B (0.037) and 4BDA (0.011), which showed that algorithms developed for deep ocean (OC3B and OC3C) have better performance than algorithms developed for inland waters (4BDA). If compared to other Brazilian tropical inland water aquatic systems, the performance of 2BDA, 3BDA and NDCI showed R^2 values higher than 0.9 during the calibration step [12]. However, for the Araruama Lagoon, the R^2 values from these three algorithms were lower than 0.003. This difference in the performance could be related to the fact that Araruama Lagoon is a hypersaline environment and the high concentration of salt in the water could be masking the results, although the R_{rs} spectra show the features of a reservoir dominated by cyanobacteria. This poor performance in the calibration of all algorithms highlights the importance of having an extreme environment as a study site in bio-optical modeling studies, since one of the goals of this field is to have an algorithm that can perform well in different aquatic systems.

The poor performance of all algorithms could be associated to the fact that none of these algorithms were developed for hypersaline aquatic systems, which make their calibration difficult in this type of environment. Another source of error could be associated to the temporal window between the image acquisition and field sampling. Since we are using ground truth data that are collected as part of a routine monthly monitoring, we could not find an exact match with temporal windows ranging from 2 to more than 10 days. This can lead to erroneous interpretations since the dynamics of parameters, mainly the biotic ones such as phytoplankton, in the water column can change within days according to the environment dynamics. Adopting a 3-days window, the calibrations showed in Table 5 improved mainly for the chl-*a* algorithms. Table 6 shows the calibrations using only the images within the 3-days window from the field campaign, which shows that EMPC got a R^2 value of 0.43, while using the entire dataset the R^2 value was around 0.08. For the turbidity estimations, the improvement was not big as for the chl-*a* estimations varying from an R^2 of 0.574 for the 1BDA using the entire dataset to an R^2 of 0.596 using only the 3-days window data. These results

Chl-a algorithms			
Name	**R^2**	**Slope**	**Intercept**
2BDA	<0.001	-0.026	14.369
3BDA	0.002	-0.256	14.270
4BDA	0.011	9.806	14.097
NDCI	0.003	7.878	12.561
OC3A	0.006	-4.510	15.753
OC3B	0.037	-16.635	21.911
OC3C	0.065	-29.037	28.519
EMPC	0.087	101.760	-98.513
Turbidity algorithms			
Name	**R^2**	**Slope**	**Intercept**
1BDA	0.574	1145.1	1.1929
2BDA	0.127	-3.5418	8.2162
LSBA	0.385	453.18	0.3646
EMPT	0.450	1.2385	3.518

Table 5. R^2, slope and intercept of the linear regression from the bio-optical algorithms tested (shaded areas represents the algorithms that were used for validation)

showed that the calibration is most affected by the temporal window when a biotic parameter is being analysed.

Chl-a algorithms			
Name	**R^2**	**Slope**	**Intercept**
4BDA	0.049	19.022	15.061
OC3A	0.223	-33.516	29.576
OC3B	0.186	-23.12	23.798
EMPC	0.430	159.3	-164.79
Turbidity algorithms			
Name	**R^2**	**Slope**	**Intercept**
1BDA	0.596	1031.2	3.054
2BDA	0.211	-3.193	10.512
LSBA	0.509	437.33	2.757
EMPT	0.304	0.890	5.550

Table 6. R^2, slope and intercept of the linear regression from the bio-optical algorithms tested using a 3 days temporal window

http://dx.doi.org/10.5772/61869

If compared to the performance of 2BDA and 3BDA for the estimation of chl-*a* in Taganrog Bay [25] the calibration for Araruama is poor, since the R^2 values found by [25] were 0.84 and 0.87 for the 2DBA and 3BDA, respectively. However, if compared to another hypersaline environment, such as Mono Lake, CA, USA, the results are equivalent since an R^2 of 0.49 was found to correlate chl-*a* and a bio-optical algorithm developed for the airborne visible/infrared imaging spectrometer (AVIRIS) sensor [54]. These results highlight the current need for a global database of bio-optical modeling data for inland waters, as well as the development of more semi- and quasi-analytical algorithms. Although few attempts have been proposed to create a global database of bio-optical modeling data for inland waters [55–56], we still need an organization such as the International Ocean Colour Coordinating Group (IOCCG) to coordinate the protocols, products and database of algorithms and bio-optical modeling data. Thus, the global bio-optical modeling of inland waters will only be achieved when we have algorithms developed and tested for all different types of environments.

4.2.2. Validation

The validation of the bio-optical algorithms with the best R^2 in the calibration was computed using two different methods: validation plots between the measured and the estimated values of chl-*a* and turbidity and error estimators. Figure 6 showed the validation plots for the four bio-optical algorithms analysed in this chapter: 4BDA (Figure 6A), OC3C (Figure 6B), OC3B (Figure 6C) and EMPC (Figure 6D). The dashed red line represents the 1:1 line where the points of the scatter plot should be over that line. In Figure 6A, we observed that the points are vertically distributed showing that there is no variation in the estimated values of log (chl-*a*); however, the error estimator showed that 4BDA has the lowest NRMSE of 24.13% among the tested algorithms. This fact showed that error estimators are only statistical and do not represent well the reality of the distribution of the data. Figure 6B and 6C showed the results for the algorithms proposed for ocean color remote sensing, OC3B and OC3C, the NRMSE for these bio-optical algorithms were 27.37% and 30.80%, respectively. The validation plots for both bio-optical algorithms showed a better distribution than the 4BDA since they showed a better distribution over the 1:1 line. However, both of the ocean color algorithms showed to underestimate (Figures 6B and 6C) the high values of log (chl-*a*). Figure 6D showed the scatter plot for the empirical algorithm (EMPC), which showed a NRMSE of 30.46%. This validation plot showed a similar pattern to the previous semi-empirical models and also underestimate the values of log (chl-*a*).

Based on these results for the chl-*a* bio-optical algorithms, we observed that although the lowest NRMSE was found in the 4BDA, the validation plots showed that the other algorithms showed a better distribution and can explain better the estimation of the log (chl-*a*). Therefore, OC3B showed the best performance with a NRMSE of 27.37% and a validation plot that underestimates the high values of chl-*a*. This underestimation was expected since for the ocean color bio-optical modeling the concentration of chl-*a* is not high and in the case of Araruama Lagoon the concentration can reach 130 μg/L of chl-*a*. As discussed in the calibration results, if compared to another tropical inland water body, the NRMSE are higher. In [12] the NRMSE founded for 2BDA, 3BDA and NDCI were 18.32%, 19.68% and 17.85%, respectively, for bio-

optical models calculated using proximal hyperspectral sensor. These differences can be related to the atmospheric correction, which is not needed for the proximal hyperspectral sensor [12], but also for the fact that Araruama Lagoon has a very unique biogeochemical cycling, which could lead to different composition of the water column. Overall, more studies should be conducted in Araruama Lagoon to better understand the optical properties in this aquatic system.

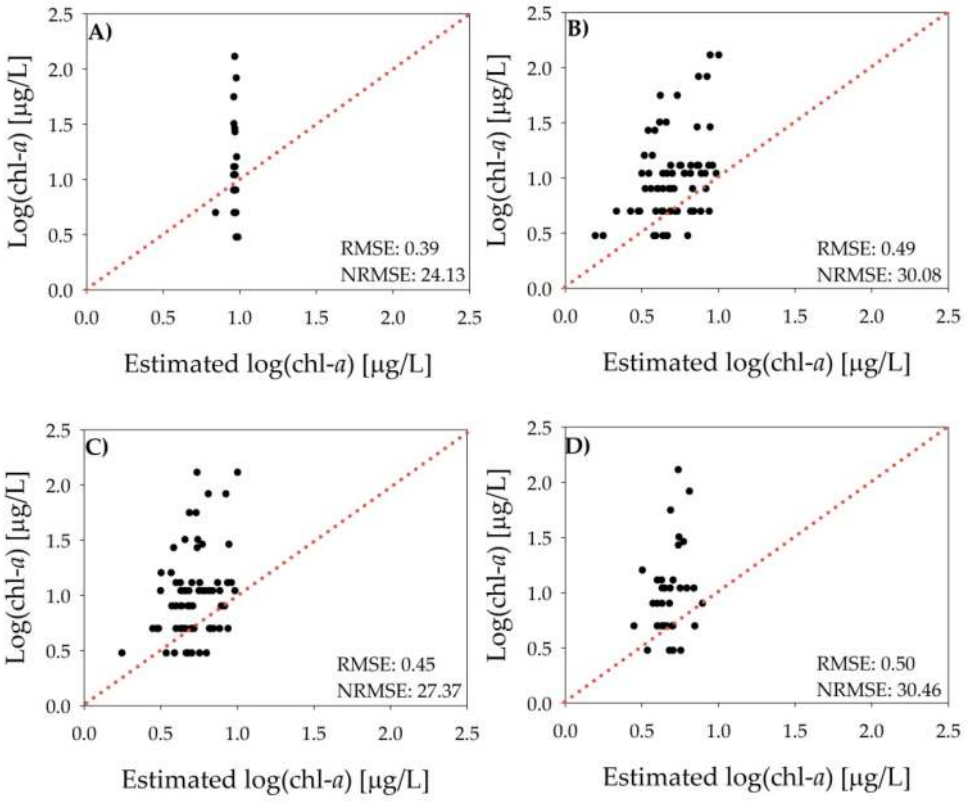

Figure 6. Validation plots for the chl-*a* bio-optical algorithms: (A) 4BDA; (B) OC3C; (C) OC3B; (D) EMPC

The validation for the turbidity bio-optical algorithms showed a better agreement between the validation plots and the error estimators. Figure 7 showed the validation plots for the four bio-optical algorithms analysed in this chapter: 1BDA (Figure 7A), 2BDA (Figure 7B), LSBA (Figure 7C) and EMPT (Figure 7D). The lowest NRMSE was 15.49% and was achieved by applying the 1BDA to the R_{rs} data (Figure 7A); the validation plot also showed most of the points close to the 1:1 line, but as well as for the chl-*a* algorithms for high values of turbidity the algorithms underestimated the values. The empirical algorithm (EMPT) had the second best NRMSE

http://dx.doi.org/10.5772/61869

(17.87%) among the turbidity bio-optical algorithms analysed and the validation plot showed to be similar to the previous algorithm. 2BDA and LSBA showed a NRMSE of 22.37% and 28.04%, respectively, which are higher than the 1BDA and EMPT algorithms. The validation plot for 2BDA and LSBA also showed a worst distribution of the scatter points and also showed an underestimation of the high values of turbidity. Overall, the performance of 1BDA showed the best validation plot and NRMSE value among the four bio-optical algorithms analysed in this chapter.

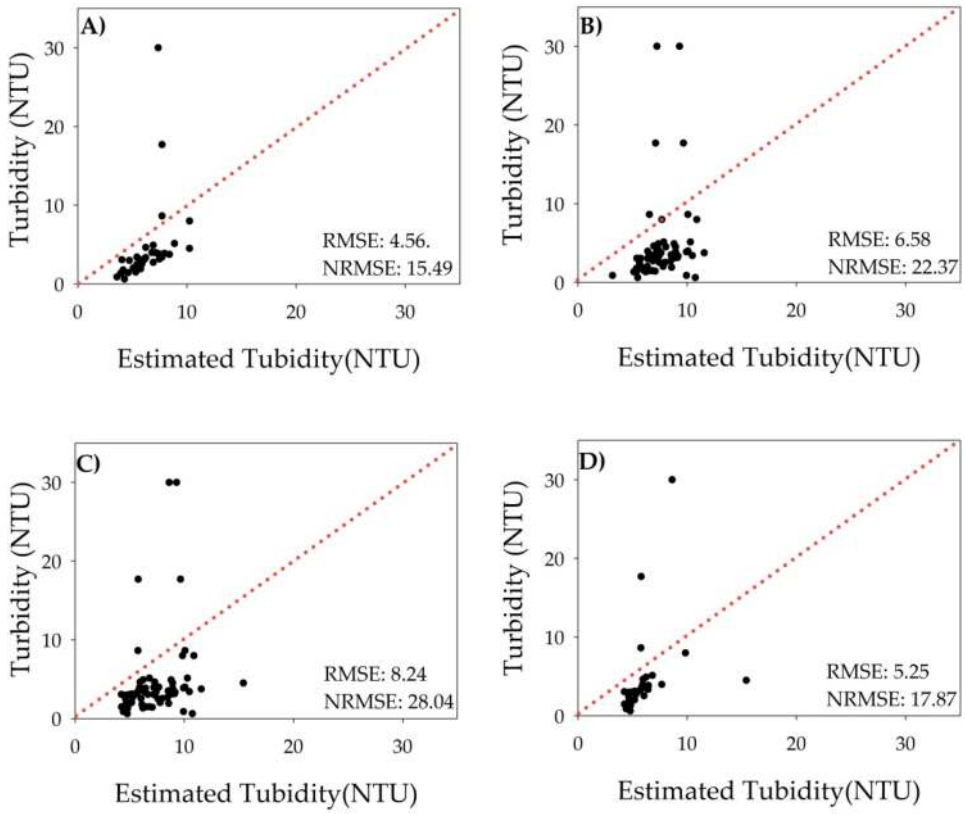

Figure 7. Validation plots for the turbidity bio-optical algorithms: (A) 1BDA; (B) 2BDA; (C) LSBA; (D) EMPT

4.3. Spatial distribution

Applications of bio-optical modeling to monitor water quality in inland waters have been increasing in the past decade, and this increase is also noticed in the public and private sector investments on remote sensing technologies to monitor water quality and quantity. The advantages of using remote sensing technologies over traditional methods to monitor water

quality parameters were already discussed in the introduction of this chapter; however, another advantage of using remote sensing is in the spatial distribution of the data. While using traditional methods of water quality monitoring computes the spatial assessment of the water quality by performing spatial interpolations or by geostatistical methods of few sampling points, remote sensing images can provide different values for each pixel within the aquatic system. The difference is that the few sampling points used to interpolate the data for the aquatic system area is now replaced for several pixels values in the image, where the interpolation is not needed; therefore, it does not have the error caused by data interpolation methods. Figure 8 shows the spatial distribution of chl-*a* and turbidity in the Araruama Lagoon where we observed that the west part of the lagoon has the highest values of chl-*a* and for the turbidity regions close to the bays have highest turbidity values. These spatial patterns are related to the hydrodynamic of the aquatic system, and the combination of bio-optical and hydrodynamic modeling [57] is a powerful tool to understand the spatial dynamics of the environment.

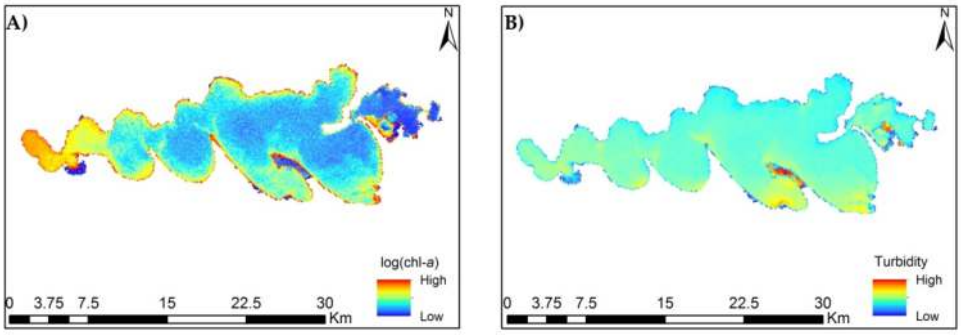

Figure 8. Application of the bio-optical algorithms to the HICO image from Araruama Lagoon acquired on August 3, 2013. (A) Application of calibrated OC3C; (B) Application of calibrated 1BDA

5. Final considerations

Based on the case study of Araruama Lagoon, we observe the need for calibration and validation of bio-optical algorithms in different inland waters since the variability of water column constituents from region to region is big. We also observe that the use of orbital hyperspectral sensors is important for the development of bio-optical modeling due to the number of spectral bands which allow us to study small features, such as the absorption peak of PC around 620 nm. Thus, narrow spectral bands can highlight specific absorption features which can be used in the development and improvement of bio-optical algorithms, mainly the semi- and quasi-analytical algorithms which are based on the radiative transfer theory. Therefore, future hyperspectral missions such as the Hyperspectral Imager SUIte (HISUI), the PRecursore IperSpettrale della Missione Applicativa (PRISMA), and the Environmental

http://dx.doi.org/10.5772/61869

Mapping and Analysis Program (EnMAP) are important for the development of bio-optical modeling.

Moreover, these new hyperspectral missions will support a global mapping of inland water quality which is only possible through multispectral sensors such as Landsat, MODIS and MERIS. However, not all water quality parameters are possible to be measured only using multispectral sensors, for example, the Landsat series which have a poor spectral resolution that does not detect the spectral features such as peaks and trough of chl-*a.* MODIS, on the other hand, have a narrow band moderate spectral resolution; however, its spatial resolution makes the monitoring of small and medium inland water bodies difficult. Therefore, the development of new global hyperspectral sensors will make the assessment of water quality through remote sensing possible because of the high spectral and spatial resolution.

Finally, our case study showed that even by developing an empirical algorithm, the semi-empirical algorithms outperform them. The best performance for chl-*a* bio-optical algorithms was found by applying OC3B (NRMSE of 27.37%) and for turbidity, the 1BDA showed the best performance with a NRMSE of 15.49%. Although the lower errors estimators validation plots (Figures 6 and 7) showed that all algorithms underestimated the high values of chl-a and turbidity, highlighting the need of different calibrations for different water types. This chapter showed a very small set of methods used in bio-optical modeling and also highlighted the need for development and improvement of bio-optical algorithms.

Acknowledgements

We thank the HICO team at Oregon State University (OSU), especially Jasmine Nahorniak for providing access to the database and to all her attention to us. C. A. S. Araújo thanks the Brazilian National Counsel of Technological and Scientific Development (CNPq) for the PCI fellowship (under the grant 300177/2015-1). M. P. Curtarelli also thanks the CNPq for the graduate scholarship (under the grant 161233/2013-9).

Author details

Igor Ogashawara[1*], Marcelo P. Curtarelli[2], Carlos A. S. Araujo[2] and José L. Stech[2]

*Address all correspondence to: igoroga@gmail.com

1 Department of Earth Sciences, Indiana University – Purdue University at Indianapolis (IUPUI), Indianapolis, IN, USA

2 Remote Sensing Division, National Institute for Space Research (INPE), São José dos Campos, SP, Brazil

References

[1] Jensen JR. Remote Sensing of the Environment: An Earth Resource Perspective. 2nd ed. Upper Saddle River, NJ: Prentice-Hall; 2007. 592 p.

[2] Mobley C. Radiative Transfer in the Ocean. In: Steele JH. (Ed.) Encyclopedia of Ocean Sciences. 1st ed. London: Academic Press; 2001. pp. 2321–2330.

[3] Platt T, Hoepffner N, Stuart V, Brown C. (Eds.) Ocean colour? The societal benefits of ocean-colour technology. Reports of the International Ocean-Colour Coordinating Group, No. 7.. 1st ed. Dartmouth, Canada: IOCCG; 2008.

[4] Cox C, Munk W. Measurement of the roughness of the sea surface from photographs of the sun's glitter. J Optic Soc Am 1954;44(11):838–50.

[5] Petzold TJ. Volume scattering functions for selected ocean waters. Ref. 72–28. San Diego, CA: Scripps Institute of Oceanography, University of California; 1972. 79 p.

[6] Jerlov NG. Optical oceanography. Elsevier Oceanographic Series, v. 5. Amsterdam: Elsevier; 1968. 194 p.

[7] Jerlov NG. Marine optics. Elsevier Oceanographic Series, v. 14. ed. Amsterdam: Elsevier; 1976. 231 p.

[8] Preisendorfer RW. Hydrologic optics. Vol. II: Foundations ed. Washington, DC: U.S. Dept. of Commerce; 1976.

[9] Gordon HR, Brown OB, Jacobs MM. Computed Relationships between the Inherent and Apparent Optical Properties of a Flat Homogeneous Ocean. Appl Optic 1975;14(2):417–27.

[10] Bukata RP, Jerome JH, Bruton JE, Jain SC. Determination of inherent optical properties of Lake Ontario coastal waters. Appl Optic 1979;18(23):3926–32.

[11] Ogashawara I. Terminology and classification of bio-optical algorithms. Remote Sens Lett 2015;6(8):613–7. DOI: 10.1080/2150704X.2015.1066523

[12] Augusto-Silva PB, Ogashawara I, Barbosa CCF, Carvalho LAS, Jorge DSF, Fornari CI, Stech JL. Analysis of MERIS reflectance algorithms for estimating chlorophyll-a concentration in a Brazilian reservoir. Remote Sens 2014;6:11689–707. DOI: 10.3390/rs61211689

[13] Matthews MW, Odermatt D. Improved algorithm for routine monitoring of cyanobacteria and eutrophication in inland and near-coastal waters. Remote Sens Environ 2015;156:374–82. DOI: 10.1016/j.rse.2014.10.010

[14] Ogashawara I, Alcantara EH, Curtarelli MP, Adami M, Nascimento RFF, Souza, AF, Stech JL, Kampel M. Performance analysis of MODIS 500-m spatial resolution products for estimating chlorophyll-a concentrations in oligo- to meso-trophic waters case

study: Itumbiara Reservoir, Brazil. Remote Sens 2014;6:1634–53. DOI: 10.3390/rs6021634

[15] Feng L, Hu C, Chen X, Qingjun S. Influence of the Three Gorges Dam on total suspended matters in the Yangtze Estuary and its adjacent coastal waters: Observations from MODIS. Remote Sens Environ 2014;140:779–88. DOI: 10.1016/j.rse.2013.10.002

[16] El-Alem A, Chokmani K, Laurion I, El-Adlouni SE. Comparative analysis of four models to estimate chlorophyll-a concentration in case-2 waters using MODerate resolution imaging spectroradiometer (MODIS) imagery. Remote Sens 2012;4:2373–400. DOI: 10.3390/rs4082373

[17] Hu C. A novel ocean color index to detect floating algae in the global oceans. Remote Sens Environ 2009;113:2118–29. DOI: 10.1016/j.rse.2009.05.012

[18] Li L, Sengpiel RE, Pascual DL, Tedesco LP, Wilson JS, Soyeux E. Using hyperspectral remote sensing to estimate chlorophyll-a and phycocyanin in a mesotrophic reservoir. Int J Remote Sens 2010;31(15):4147–62. DOI: 10.1080/01431161003789549

[19] Li L, Li L, Song K, Li Y, Tedesco LP, Shi K, Li Z. An inversion model for deriving inherent optical properties of inland waters: Establishment, validation and application. Remote Sens Environ 2013;135:150–66. DOI: 10.1016/j.rse.2013.03.031

[20] Olmanson LG, Brezonik PL, Bauer ME. Airborne hyperspectral remote sensing to assess spatial distribution of water quality characteristics in large rivers: The Mississippi River and its tributaries in Minnesota. Remote Sens Environ 2013;130:254–65. DOI: 10.1016/j.rse.2012.11.023

[21] Hu C, Feng L, Lee L, Davis CO, Mannino A, McClain CR, Franz BA. Dynamic range and sensitivity requirements of satellite ocean color sensors: Learning from the past. Appl Optic 2012;51(25):6045–62. DOI: 10.1364/AO.51.006045

[22] Cho HJ, Ogashawara I, Mishra D, White J, Kamerosky A, Morris L, Clarker C, Simpson A, Banisakher D. Evaluating Hyperspectral Imager for the Coastal Ocean (HICO) data for seagrass mapping in Indian River Lagoon, FL. GISci Remote Sens 2014;51:120–38. DOI: 10.1080/15481603.2014.895577

[23] Gao BC, Li RR. Removal of think cirrus scattering effects for remote sensing of ocean color from space. IEEE Geosci Remote Sens Lett 2012;9:972–6. DOI: 10.1109/LGRS.2012.2187876

[24] Ryan JP, Davis CO, Tufllaro NB, Kudela RM, Gao BC. Application of the hyperspectral imager for the coastal ocean to phytoplankton ecology studies in Monterey Bay, CA USA. Remote Sens 2014;6:1007–25. DOI: 10.3390/rs6021007

[25] Moses WJ, Gitelson AA, Berdnikov S, Bowles JH, Povazhnyi V, Sapryngin V, Wagner EJ, Patterson KW. HICO-based NIR-red models for estimating chlorophyll-a concentration in productive coastal waters. IEEE Geosci Remote Sens Lett 2014;11(6):1111–5. DOI: 10.1109/LGRS.2013.2287458

[26] Kudela RM, Palacios SL, Austerberry DC, Accorsi EK, Guild LS, Torres-Perez JL. Application of hyperspectral remote sensing to cyanobacterial blooms in inland waters. Remote Sens Environ 2015;167:196–205. DOI: 10.1016/j.rse.2015.01.025

[27] Duan H, Ma R, Xu J, Zhang Y, Zhang B. Comparison of different semi-empirical algorithms to estimate chlorophyll-a concentration in inland lake water. Environ Monitor Assess 2010;170:231–44. DOI: 10.1007/s10661-009-1228-7

[28] Instituto Brasileiro de Geografia e Estatística (IBGE). Demographic Census [Internet]. 2010. Available from: http://www.ibge.gov.br/home/estatistica/populacao/censo2010/ [Accessed: 01 Sep 2015]

[29] Kjerfve B, Schettini CAF, Knoppers B, Lessa G, Ferreira HO. Hydrology and salt balance in a large, hypersaline coastal lagoon: Lagoa de Araruama, Brazil. Estuarine, Coastal Shelf Sci 1996;42:701–25.

[30] Braga CZF, Vianna ML, Kjerfve B. Environmental characterization of a hypersaline coastal lagoon from Landsat-5 Thematic Mapper data. Int J Remote Sens 2003;24:3219–34. DOI: 10.1080/0143116031000075099

[31] Peel MC, Finlayson BL, McMahon TA. Updated world map of the Köppen-Geiger climate classification. Hydrol Earth System Sci 2007;11:1633–44. DOI: 10.5194/hess-11-1633-2007

[32] Empresa Brasileira de Pesquisa Agropecuária (EMBRAPA). Brazilian climatic database [Internet]. 2003. Available from: http://www.bdclima.cnpm.embrapa.br/ [Accessed: 01 Sep 2015]

[33] Mello TBM. Caracterização Biogeoquímica da Lagoa de Araruama, RJ [thesis]. Niterói: Universidade Federal Fluminense - Instituto de Química; 2007. 82 p. [in Portuguese]

[34] Lamparelli MC. Grau de trofia em corpos d'água do estado de São Paulo: avaliação dos métodos de monitoramento [dissertation]. São Paulo: São Paulo University - Department of Ecology; 2004. 235 p. [in Portuguese]

[35] Comitê de Bacias Lagos São João. Phytoplankton monitoring of the Araruama Lake [Internet]. 2012. Available from: http://www.lagossaojoao.org.br/nc-relatorioqualiaguas.htm [Accessed: 25 Aug 2015] [in Portuguese]

[36] Comitê de Bacias Lagos São João. Monthly water quality Report [Internet]. 2014. Available from: http://www.lagossaojoao.org.br/nc-relatorioqualiaguas.htm [Accessed: 25 Aug 2015] [in Portuguese]

[37] Oregon State University. HICO - Hyperspectral Imager for the Coastal Ocean [Internet]. 2015. Available from: http://hico.coas.oregonstate.edu/ [Accessed: 01 Sep 2015]

[38] Gao BC, Montes MJ, Ahmad Z, Davis CO. Atmospheric correction algorithm for hyperspectral remote sensing of ocean color from space. Appl Optic 2000;39(6):887–96. DOI: 10.1364/AO.39.000887

[39] Gao BC, Goetz AFH. Column atmospheric water vapor and vegetation liquid water retrievals from airborne imaging spectrometer data. J Geophys Res 1990;95(D4):3549–64. DOI: 10.1029/JD095iD04p03549

[40] Dall'Olmo G, Gitelson AA. Effect of bio-optical parameter variability on the remote estimation of chlorophyll-a concentration in turbid productive waters: Experimental results. Appl Optic 2005;44:412–22. DOI: 10.1364/AO.44.000412

[41] Gitelson AA, Gritz U, Merzlyak MN. Relationships between leaf chlorophyll content and spectral reflectance and algorithms for non-destructive chlorophyll assessment in higher plant leaves. J Plant Physiol 2003;160:271–82. DOI: 10.1078/0176-1617-00887

[42] Le C, Li Y, Zha Y, Sun D, Huang C, Lu H. A four-band semi-analytical model for estimating chlorophyll a in highly turbid lakes: The case of Taihu Lake, China. Remote Sens Environ 2009;113:1175–82. DOI: 10.1016/j.rse.2009.02.005

[43] Mishra S, Mishra DR. Normalized difference chlorophyll index: A novel model for remote estimation of chlorophyll-a concentration in turbid productive waters. Remote Sens Environ 2012;117:394–406. DOI: 10.1016/j.rse.2011.10.016

[44] NASA Ocean Biology Processing Group. Ocean Color Chlorophyll (OC) v6 [Internet]. 18 Mar 2010. Available from: http://oceancolor.gsfc.nasa.gov/REPROCESSING/R2009/ocv6/ [Accessed: 02 Sep 2015]

[45] Doxaran D, Babin DM, Leymarie E. Near-infrared light scattering by particles in coastal waters. Optics Exp 2007;15:12834–49. DOI: 10.1364/OE.15.012834

[46] Doxaran D, Froidefond JM, Castaing P, Babin M. Dynamics of the turbidity maximum zone in a macrotidal estuary (the Gironde, France): Observations from field and MODIS satellite data. Estuar Coastal Shelf Sci 2009;81(3):321–32. DOI: 10.1016/j.ecss.2008.11.013

[47] Zhang Y, Lin S, Liu J, Qian X, Ge Y. Time-series MODIS image-based retrieval and distribution analysis of total suspended matter concentrations in Lake Taihu (China). Int J Environ Res Public Health 2010;7(9):3545–60. DOI: 10.3390/ijerph7093545

[48] Ogashawara I, Curtarelli MP, Souza AF, Augusto-Silva PB, Alcântara EH, Stech JL. Interactive correlation environment (ICE) — a statistical web tool for data collinearity analysis. Remote Sens 2014;6:3059–74. DOI: 10.3390/rs6043059

[49] Hidrosfera INPE. ICE - Interactive Correlation Environment [Internet]. 2014. Available from: http://www.dsr.inpe.br/hidrosfera/ice/ [Accessed: 02 Sep 2015]

[50] Gitelson AA, Yacobi YZ, Schalles JF, Rundquist DC, Han L, Stark R, Etzion D. Remote estimation of phytoplankton density in productive waters. Arch Hydrobiol 2000;55:121–36.

[51] Ogashawara I, Mishra DR, Mishra S, Curtarelli MP, Stech JL. A performance review of reflectance based algorithms for predicting phycocyanin concentrations in inland waters. Remote Sens 2013;5:4774–98. DOI: 10.3390/rs5104774

[52] Dekker AG. Detection of Optical Water Quality Parameters for Eutrophic Waters by High [dissertation]. Amsterdam, the Netherlands: Vrije Universiteit; 1993.

[53] Gitelson AA. The peak near 700 nm on radiance spectra of algae and water: relationships of its magnitude and position with chlorophyll concentration. Int J Remote Sens 1992;13(17):3367–73. DOI: 10.1080/01431169208904125

[54] Melack JM, Gastil M. Airborne remote sensing of chlorophyll distributions in Mono Lake, California. Hydrobiologia 2001;466:31–8.

[55] GloboLakes. GloboLakes - Global Observatory of Lake Responses to Environmental Change [Internet]. [Updated: 2014]. Available from: http://www.globolakes.ac.uk/ [Accessed: 02 Sep 2015]

[56] GEO. Group on Earth Observations [Internet]. [Updated: 2015]. Available from: https://www.earthobservations.org/index.php [Accessed: 02 Sep 2015]

[57] Curtarelli MP, Ogashawara I, Alcântara EH, Stech JL. Coupling remote sensing bio-optical and three-dimensional hydrodynamic modeling to study the phytoplankton dynamics in a tropical hydroelectric reservoir. Remote Sens Environ 2015;157:185–98. DOI: 10.1016/j.rse.2014.06.013